

# Impact of particles on the *Planck* HFI detectors: Ground-based measurements and physical interpretation

A. Catalano<sup>1</sup>, P. Ade<sup>2</sup>, Y. Atik<sup>3</sup>, A. Benoit<sup>4</sup>, E. Bréee<sup>5</sup>, J.J. Bock<sup>6,7</sup>, P. Camus<sup>4</sup>, M. Chabot<sup>8</sup>, M. Charra<sup>3</sup>, B.P. Crill<sup>7</sup>, N. Coron<sup>3</sup>, A. Coulais<sup>9</sup>, F.-X. Désert<sup>10</sup>, L. Fauvet<sup>11</sup>, Y. Giraud-Héraud<sup>5</sup>, O. Guillaudin<sup>1</sup>, W. Holmes<sup>7</sup>, W. C. Jones<sup>12</sup>, J.-M. Lamarre<sup>9</sup>, J. Macías-Pérez<sup>1</sup>, M. Martinez<sup>3</sup>, A. Miniussi<sup>3</sup>, A. Monfardini<sup>4</sup>, F. Pajot<sup>3</sup>, G. Patanchon<sup>5</sup>, A. Pelissier<sup>1</sup>, M. Piat<sup>5</sup>, J.-L. Puget<sup>3</sup>, C. Renault<sup>1</sup>, C. Rosset<sup>5</sup>, D. Santos<sup>1</sup>, A. Sauvé<sup>13</sup>, L.D. Spencer<sup>2</sup>, and R. Sudiwala<sup>2</sup>

<sup>1</sup> Laboratoire de Physique Subatomique et de Cosmologie, CNRS/IN2P3, Université Joseph Fourier Grenoble I, Institut National Polytechnique de Grenoble, 53 rue des Martyrs, 38026 Grenoble Cedex, France

<sup>2</sup> School of Physics and Astronomy, Cardiff University, Queens Buildings, The Parade, Cardiff, CF24 3AA, UK

<sup>3</sup> Institut d’Astrophysique Spatiale, CNRS (UMR8617) Université Paris-Sud 11, Bâtiment 121, Orsay, France

<sup>4</sup> Institut Néel, CNRS, Université Joseph Fourier Grenoble I, 25 rue des Martyrs, Grenoble, France

<sup>5</sup> Astroparticule et Cosmologie, CNRS (UMR 7164), Université Denis Diderot Paris 7, Bâtiment Condorcet, 10 rue A. Domon et Leonie Duquet, Paris, France

<sup>6</sup> California Institute of Technology, Pasadena, California, USA

<sup>7</sup> Jet Propulsion Laboratory, California Institute of Technology, 4800 Oak Grove Drive, Pasadena, California, USA

<sup>8</sup> IPN: Institut de Physique Nucléaire, CNRS/IN2P3, Université Paris-Sud 11, 91406 Orsay cedex, France

<sup>9</sup> LERMA, CNRS, Observatoire de Paris, 61 avenue de l’Observatoire, Paris, France

<sup>10</sup> IPAG: Institut de Planétologie et d’Astrophysique de Grenoble, Université Joseph Fourier, Grenoble 1/CNRS-INSU, UMR 5274, 38041 Grenoble, France

<sup>11</sup> European Space Agency, ESTEC, Keplerlaan 1, 2201 AZ Noordwijk, The Netherlands

<sup>12</sup> Department of Physics, Princeton University, Princeton, New Jersey, USA

<sup>13</sup> CNRS, IRAP, 9 Av. colonel Roche, BP 44346, 31028 Toulouse Cedex 4, France

Preprint online version: March 27, 2014

## ABSTRACT

The *Planck* High Frequency Instrument (HFI) surveyed the sky continuously from August 2009 to January 2012. Its noise and sensitivity performance were excellent, but the rate of cosmic ray impacts on the HFI detectors was unexpectedly high. Furthermore, collisions of cosmic rays with the focal plane produced transient signals in the data (“glitches”) with a wide range of characteristics. A study of cosmic ray impacts on the HFI detector modules has been undertaken to categorize and characterize the glitches, to correct the HFI time-ordered data, and understand the residual effects on *Planck* maps and data products. This paper presents an evaluation of the physical origins of glitches observed by the HFI detectors. In order to better understand the glitches observed by HFI in flight, several ground-based experiments were conducted with flight-spare HFI bolometer modules. The experiments were conducted between 2010 and 2013 with HFI test bolometers in different configurations using varying particles and impact energies. The bolometer modules were exposed to 23 MeV protons from the Orsay IPN TANDEM accelerator, and to <sup>241</sup>Am and <sup>244</sup>Cm  $\alpha$ -particle and <sup>55</sup>Fe radioactive X-ray sources. The calibration data from the HFI ground-based preflight tests were used to further characterize the glitches and compare glitch rates with statistical expectations under laboratory conditions. Test results provide strong evidence that the dominant family of glitches observed in flight are due to cosmic ray absorption by the silicon die substrate on which the HFI detectors reside. Glitch energy is propagated to the thermistor by ballistic phonons, while there is also a thermal diffusion contribution. The implications of these results for future satellite missions, especially those in the far-infrared to sub-millimetre and millimetre regions of the electromagnetic spectrum, are discussed.

**Key words.** instrumentation: detectors – space vehicles: instruments – methods: data analysis – cosmic rays – cosmic background radiation

## 1. Introduction

The *Planck* mission (Planck Collaboration (2013 results I) 2014)<sup>1</sup> has observed the sky between August 2009 and August 2013 in the frequency range from 30 GHz to 1 THz from its

Send offprint requests to: A. Catalano - catalano@lpsc.in2p3.fr

<sup>1</sup> *Planck* (<http://www.esa.int/Planck>) is a project of the European Space Agency (ESA) with instruments provided by two scientific consortia funded by ESA member states (in particular the lead countries France and Italy), with contributions from NASA(USA) and telescope reflectors provided by a collaboration between ESA and a scientific consortium led and funded by Denmark.

orbital vantage point about the second Sun-Earth Lagrange point (L2). The *Planck* satellite comprises a telescope, a service module, and two instruments: the High Frequency Instrument (HFI) and the Low Frequency Instrument (LFI). The HFI operates with 52 high impedance bolometers cooled to 100 mK in a range of frequencies between 100 GHz and 1 THz, and shows an unprecedented photon sensitivity within its frequency bands (Planck Collaboration (early results IV) 2011). At the same time, however, the HFI detectors exhibit a strong coupling with cosmic-ray radiation that produces transient glitches in the raw time-ordered information (TOI). The data affected by large-amplitude glitches are rendered unusable for science, and

must be masked in subsequent data processing. The redundancy of *Planck*'s scanning strategy ensures complete sky coverage even after large-amplitude glitch masking (Planck Collaboration (2013 results X) 2014; Planck Collaboration (early results VI) 2011). Smaller-amplitude glitches are flagged and the data are corrected by the subtraction of a parametric fit to an HFI glitch template. Even smaller glitches could remain hidden within the TOI noise, yielding an additional non-Gaussian systematic effect. Therefore, a proper understanding and careful data processing of the glitches are essential to meet the precision cosmology goals of the *Planck* mission. Uncorrected glitches can influence the estimation of the cosmic microwave background (CMB) angular power spectrum; in particular, there is a potential confusion between glitch residuals and the non-Gaussian features caused by topological defects or inflation processes (Masi et al. 2010).

This work, together with a companion article (Planck Collaboration (2013 results X) 2014), provides an improved understanding of the physical origin of the glitches observed in the HFI instrument in-flight data. This paper discusses several ground-based experiments using the collision of protons and  $\alpha$ -particles with spare HFI bolometers. These experiments provide better control of the incident particle characteristics (e.g., particle type, energy, impact location) and environmental conditions than the HFI in-flight data.

This article is structured as follows: we first give a short review of the cosmic-ray flux at the second Sun-Earth Lagrange point (L2). In Sect. 3 we describe the geometrical and thermal characteristics of the elements that constitute an HFI bolometer module. In Sect. 4 we summarize the results obtained from the analysis of the glitches in the HFI in-flight data. In Sect. 5 we show the results of the ground characterization of the HFI spare bolometers, and describe several radiation tests with protons and  $\alpha$ -particles. In conclusion we discuss the physical interpretation of the glitches seen by HFI in flight and the lessons learnt for future cosmological space missions.

## 2. Cosmic rays at the second Lagrange point

Cosmic rays (CRs) at L2 are composed of about 89 % protons, 10 %  $\alpha$ -particles, and 1 % nuclei of heavier elements; less than 1 % are electrons (see, e.g., Mewaldt et al. 2010; Leske et al. 2011). The most important contribution (in terms of both energy and quantity) to the CRs at L2 comes from within our own Galaxy. The incoming charged particles are modulated by the solar wind, which decelerates and partially shields the inner solar system from lower-energy galactic CRs. There is a significant anticorrelation between solar activity and the flux of CRs with energies below 10 GeV.

Besides deflecting galactic CRs, the Sun is itself a source of cosmic ray nuclei and electrons that are accelerated by shock waves travelling through the corona, and by magnetic energy released in solar flares. The typical energy reached in solar particle is of the order of keV. On the other hand, during a solar flare, the maximum energy reached is typically 10 to 100 MeV, occasionally reaching 1 GeV (roughly once a year) to 10 GeV (roughly once a decade). During the *Planck* mission, we observed 13 solar flares; each solar flare lasted a few hours and produced a change in temperature of the whole bolometer plate affecting the working point of the bolometers. The data related to these events are flagged and excluded from standard HFI data processing, so we will not consider this source of CRs here.

A third population of CRs, referred as *anomalous cosmic rays* (ACR), consists primarily of photoionized interstellar hydrogen nuclei that are accelerated at the termination shock in the

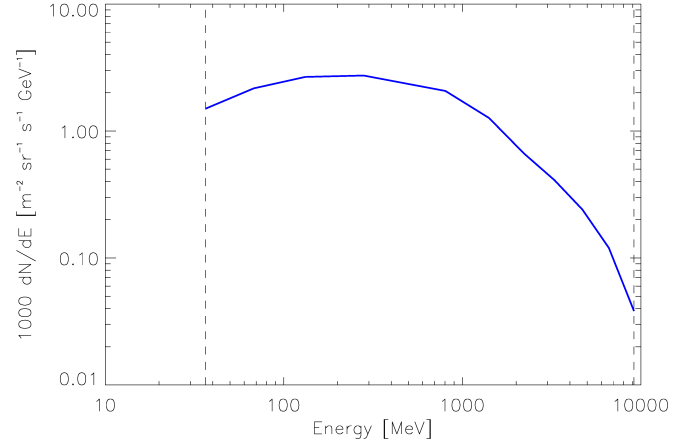


**Fig. 1.** Energy distribution of CR protons at L2. The vertical dashed lines represent the range of energies of interest for HFI (from 35 MeV to 10 GeV).

heliosphere (Stone 2012). Although heavier elements are present in the ACR population, protons with energies from hundreds of keV to 100 MeV represent a marginal component of the cosmic ray flux affecting the *Planck* HFI.

The flux of CRs is monitored onboard the *Planck* satellite by the Standard Radiation Environment Monitor (SREM)<sup>2</sup> mounted on the exterior of the spacecraft. Solar flares provided a useful test to correlate the signal measured on the outside of the spacecraft with the SREM with signals due to particle impact on HFI. We found that only CRs with energies above 39 MeV can penetrate the focal plane unit (FPU) box (Planck Collaboration (2013 results X) 2014).

We conclude that the flux of particles that can cause glitches in the HFI data is composed of protons in a range of energies between 39 MeV and 10 GeV. The energy distribution of protons is presented in Fig. 1 (Adriani et al. 2011; Christian et al. 2011; Picozza et al. 2011). Below 39 MeV, protons do not have enough energy to penetrate the FPU box to reach the 100 mK stage. The total flux of CRs peaks around 200 MeV, giving a total proton flux of 3000–4000 particles  $\text{m}^{-2} \text{sr}^{-1} \text{s}^{-1} \text{GeV}^{-1}$ .

## 3. HFI bolometers

In this section we describe the different elements that constitute an HFI bolometer module. In general, each element of a bolometer module can interact with CRs and, through the thermal link with the thermistor, it can generate a glitch in the data. One of the goals of this article is to isolate the elements of an HFI bolometer that can have an impact on the HFI data.

The HFI high-impedance bolometers (Holmes et al. 2008) are manufactured using silicon nitride supported metal-mesh absorbers and neutron transmutation doped (NTD) germanium thermistors with a resistance strongly dependent on the temperature. The use of an absorber with a spider-web shape strongly reduces the cross sectional area (of the order of 95 %) for CR and particle collisions and it was a design consideration for

<sup>2</sup> SREM consists of three detectors (Diodes D1, D2, D3) in two detector head configurations (Mohammadzadeh et al. 2003). A total of 15 discriminator levels are available to bin the energy of the detected events.

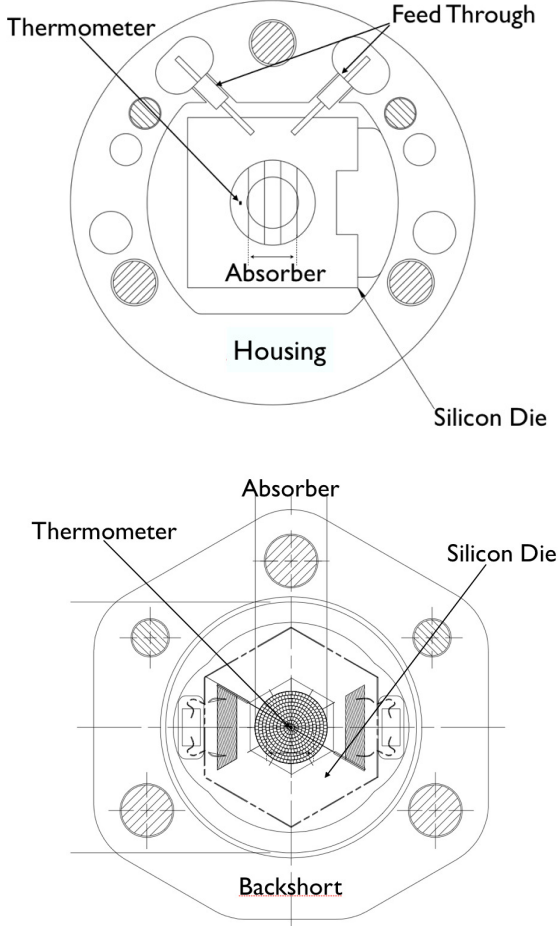


**Fig. 2.** *Top:* front perspective mechanical drawing of a polarization-sensitive bolometer (PSB). The illustration shows the forward/upper portion, i.e., PSBa, of the PSBa/b pair. The orientation of the PSBb absorber is orthogonal to the PSBa. *Bottom:* mechanical drawing of a spider-web bolometer (SWB). In both figures, the printed wiring board (PWB) and cover are not shown.

detectors intended for on-orbit and balloon-borne applications. At the same time, the effective in-band cross sectional surface area is comparable to that of a solid absorber; thus, the spider-web absorber technology reduces the CR and out-of band noise produced in the TOI data. For reviews of the theory of high-impedance bolometers see [Jones \(1953\)](#), [Mather \(1982\)](#), [Mauskopf \(1997\)](#), [Sudiwala et al. \(2000\)](#), and [Vaillancourt \(2005\)](#).

The size and grid spacing of the mesh is adapted to operate in six separated frequency bands between 100 and 857 GHz. In flight, four spider-web bolometers (SWBs) in each of five bands from 143 to 857 GHz measure the total intensity of incident radiation. In addition, eight polarization-sensitive bolometers (PSBs) in each of four bands (100, 143, 217, and 353 GHz) couple only to a single linear polarization and thus measure a linear combination of Stokes parameters  $I$ ,  $Q$ , and  $U$ . PSBs are arranged in pairs sensitive to orthogonal polarizations. Bolometer performance strongly depends on the read-out electronics design ([Catalano et al. 2010](#)). The electronics chain implemented in the HFI is an evolution of the square-wave-biased AC readout

([Rieke et al. 1989](#); [Gaertner et al. 1997](#)), known to improve the low-frequency stability of bolometers.

The elements of an HFI bolometer module are:

- *Thermometer*: the bolometer temperature is measured using an NTD germanium semiconducting thermistor. The size of the NTD thermometers is the same in all the SWBs and PSBs; it is  $30$  (thickness)  $\times 100 \times 300 \mu\text{m}$ .
- *Absorber*: the millimetre-wave absorber for SWBs and PSBs is a free standing metallized  $\text{Si}_3\text{N}_4$  micromesh supported by  $\text{Si}_3\text{N}_4$  beams. The width of the micromesh varies with the HFI band-frequency; it is between  $5$  and  $10 \mu\text{m}$ . The  $1 \mu\text{m}$  thickness of the  $\text{Si}_3\text{N}_4$  structures is the same in all the bolometers. In the PSBs, the grid spacing, always  $> 50 \mu\text{m}$ , is chosen so that it absorbs millimetre-waves with high efficiency but has a much smaller physical surface area, significantly reducing the cross section to cosmic ray particles and shorter-wavelength photons.
- *Silicon Die*: a silicon wafer of an initial diameter of  $15.2 \text{ cm}$ , diced differently for SWBs and PSBs (see Fig. 2). A  $\text{Si}_3\text{N}_4$  film of  $1 \mu\text{m}$  was deposited on both sides of the wafer. Gold with a titanium adhesion layer was deposited and patterned on the side of the wafer to define the millimetre-wave absorber, the thermal link to the absorber, and the thermalization bars and contact pads for wire bonding and the indium bump bonds. The bolometer die is located over the backshort (or the housing for the forward PSBs) and glued with epoxy. The silicon die thickness is  $350 \mu\text{m}$  in all the bolometers and the surface area is between  $0.4$  and  $0.8 \text{ cm}^2$  depending on the working frequency.
- *Backshort*: made of beryllium-copper, it supports the silicon die and it permits an optimal absorption of photons by the grid as a result of the  $\lambda/4$  relief machined into it. It is present in SWB bolometers and in the rear PSBs (PSBb).
- *Housing*: made of beryllium-copper, it supports the silicon die of the PSBa bolometers.
- *Printed wiring board (PWB)*: the PWB is mounted in the bolometer module on the opposite side of the backshort from the bolometer and it contains surface mount inductors and a ground plane that, with the capacitors and bolometer, forms a filter to attenuate radio-frequency signals before it is rectified at the bolometer.
- *Feed-through*: this element is only present in the forward bolometers of a PSB module (PSBa). It electrically links the gold pad of the forward PSB to the module PWB with a very low level of electrical cross-talk with the backward PSB (PSBb). This is achieved by using an aluminium cylinder glued with epoxy in the backshort of the backward PSB. Inside the aluminium the wire is suspended with epoxy.
- *Cover*: the cover is made of beryllium-copper. It is installed onto the backshort to protect the PWB and to support a connector.

#### 4. HFI in-flight glitches

The structure and the evolution of the in-flight glitches have been discussed in [Planck Collaboration \(early results VI\) \(2011\)](#) and the companion article [Planck Collaboration \(2013 results X\) \(2014\)](#). In this section we summarize the principal observed characteristics of the in-flight HFI glitches.

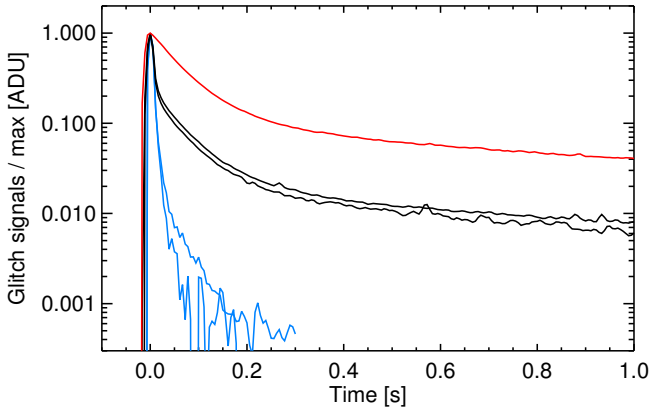
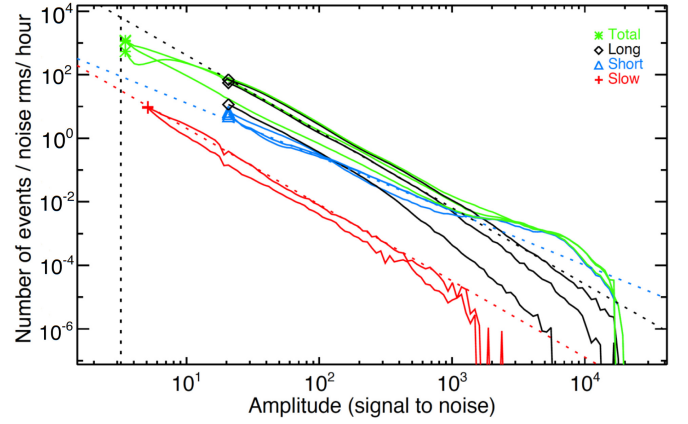
We describe the glitches observed by HFI in terms of three characteristics: 1) rate of events and its evolution during the mission; 2) characteristic event profile (glitch template); 3) the absorbed energy distribution.

**Table 1.** Summary of the ground-based bolometer tests

	TANDEM acc. Tests	$\alpha$ Test 1	$\alpha$ Test 2	HFI Ground Cal.
Location	IPN, Paris	Néel Institute, Grenoble	IAS, Paris	CSL, Liège
Period	Dec 2010	Nov 2011–Apr 2013	Jun–Nov 2011	Jun–Jul 2008
Source	TANDEM accelerator $p^+$ at 23 MeV	$^{55}\text{Fe}$ isotope source (X-rays 5.9 keV) $^{244}\text{Cm}$ source ( $\alpha$ particle at 5.9 MeV)	$^{241}\text{Am}$ source (3 Bq) $\alpha$ particles at 5.4 MeV	Secondary CR emission
Cryostat	Néel 100 mK dilution	Néel 100 mK dilution	IAS 100 mK dilution	HFI Cryostat
Detectors	3 SWB	1 SWB, 1 PSB	1 SWB, 1 PSB	52 HFI flight bol.
Read-Out El.	AC biased (same as HFI)	AC biased (same as HFI)	DC (dig. at 5 kHz)	HFI AC biased

**Table 2.** Energy absorbed [keV] in the different elements of a bolometer module for normally incident particles

Particle	NTD	Grid	Silicon die	Feed-through
30 MeV–10 GeV $p^+$ (CR@L2)	14.7–75.8	0.5–4.7	118–640	200–1000
23 MeV $p^+$ (TANDEM acc.)	137	6.5	1600	Not reached
5.9 MeV $\alpha$ ( $^{244}\text{Cm}$ )	Stopped	890	Stopped	Not reached
5.4 MeV $\alpha$ ( $^{241}\text{Am}$ )	Stopped	950	Stopped	Not reached


**Fig. 3.** HFI flight results: average short glitch template (blue), long glitch template (black), and slow glitch template (red) for one PSB in-flight bolometer (Planck Collaboration (2013 results X) 2014).

**Fig. 4.** HFI flight results: glitch energy distribution for the three families of glitches with respect to the peak amplitude, in signal-to-noise units, for three different PSB and SWB in-flight bolometers (Planck Collaboration (2013 results X) 2014). The blue line is for the short glitch population, black is for long, red is for slow, and green is for total. Power laws are shown for comparison as dashed lines.

- *Rate*: The evolution of the glitch rate is strongly correlated with the SREM as discussed in Sect. 2. This is evidence that glitches are produced by CRs and not by local phenomena such as vibrations or read-out electronics noise. The measured in-flight glitch rate was about 20 times larger than expected from the coupling between the absorber and the CRs at L2. A phenomenon other than the direct interaction of the CRs with the absorber and NTD has to be invoked to explain this (see Planck Collaboration (2013 results X) 2014). Two hypotheses have been put forward: (1) the NTD thermometer is sensitive to a change in temperature of other (larger) elements; (2) a large fraction of the glitches come from indirect interaction between CRs and bolometers, for example, protons which interact very close to the surfaces of materials surrounding the NTD+Grid (in particular copper) produce electron showers able to propagate to the absorber+NTD.
- *Shape*: From data reduction (Planck Collaboration (2013 results X) 2014), we distinguished three families of glitches with different shapes (see Fig 3): short, long, and slow

glitches. We can fit each family with a template which is the sum of first-order low-pass filters:

$$\text{template} = \sum_{i=1}^N A_i \cdot \exp(-t/\tau_i) \quad (1)$$

Short glitches present a fast decay (between 4 and 10 ms depending on the bolometer) and a tail with an amplitude of a few percent of the maximum. Long glitches present the same fast decay as the short ones but a large (about 10 %) relative amplitude tail showing intermediate to long time-constants of tens of milliseconds and about 1 s. Slow glitches show the same slow time-constants as the long and short glitches but not the fast decay. The residual glitch signal after template subtraction is significantly reduced. Indeed, the remaining contamination from glitches is below the instrumental noise level, even for channels with the highest glitch rates.

- *Spectrum*: The glitch energy distribution has been estimated for short, long, and slow glitches. The distributions can be fitted by power-laws with different indices, and differ-



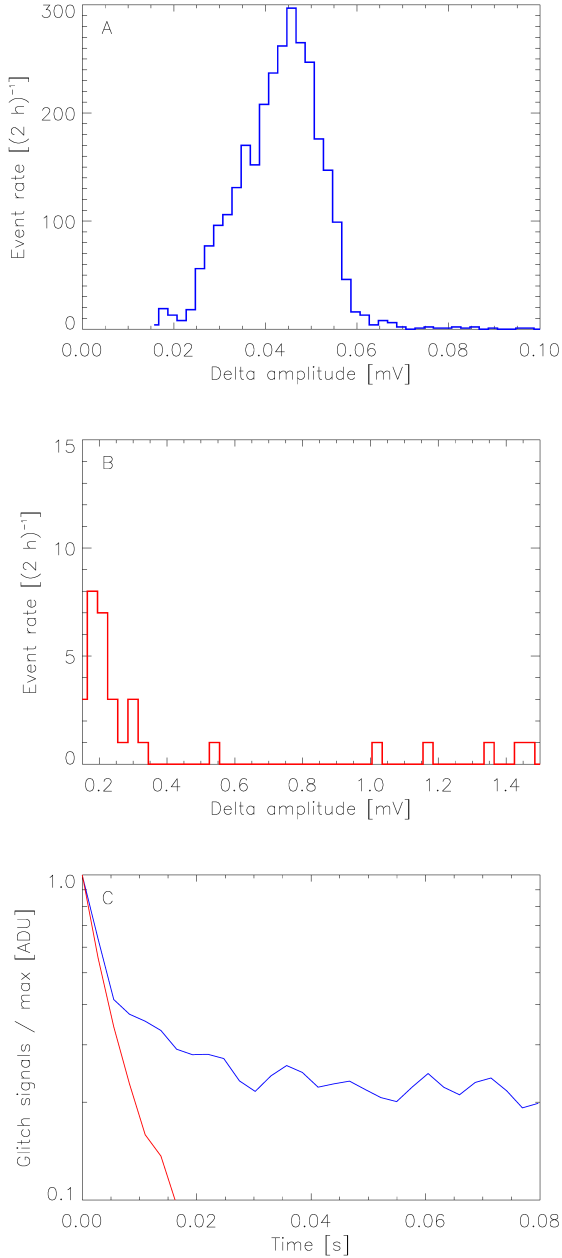


**Fig. 5.** TANDEM accelerator test. (A) Histograms of the glitch amplitudes in 2 h of integration time for low amplitudes (0 V – 0.1 mV). (B) Histograms of the glitch amplitudes in 2 h of integration for high amplitudes (greater than 0.1 mV). (C) Glitch template built by stacking all the events of the first family centered at  $45 \mu\text{V}$  (blue) and the family centered at 0.15 mV (red). Both templates show the same fast time-constant  $\tau$  (4 ms) and the blue template shows a slower time-constant (about 20 ms) with an amplitude relative to the peak of few percent.

ent bolometers show very similar results. In Fig. 4, we present the averaged energy spectra of the in-flight PSBs at 217 GHz collected during the full mission. The total number of glitches is dominated by long glitches at low absorbed energies. Short glitches dominate for high absorbed energies. Slow glitches are present only on the PSBa bolometers. Long and slow glitches show the same power law index. The short

glitches distribution shows a double structure with an elevated bump in the high energy range.

## 5. Ground measurements

For an improved understanding of the origins of the glitches seen in HFI flight data, we performed several ground-based tests on spare HFI bolometers between late 2010 and Spring 2013. The aim of the tests was to obtain a more complete view of the physical origin of the different families of glitches. These tests were performed in different configurations using 23 MeV protons from a TANDEM accelerator<sup>3</sup> and two radioactive  $\alpha$  particle sources ( $^{241}\text{Am}$  and  $^{244}\text{Cm}$ ). In addition, we used the HFI ground calibration data to check the impact of the cosmic rays at sea level with HFI bolometers. The sensitivity reached for these tests was about  $10 \text{ nV Hz}^{1/2}$ , very close to the flight performance. A list of all the tests that were performed is presented in Table 1.

We started by placing spare HFI SWBs in front of a TANDEM accelerator with a proton beam able to cover the full surface of the bolometer module. The results of this test showed that we are able to reproduce short and long glitches observed in flight without any delta-electron<sup>4</sup> production process. Because of the limited integration time during the TANDEM test, we performed other tests with  $\alpha$  sources in order to investigate more deeply the production of long glitches by using a collimated beam able to interact with small parts of the bolometer module on each test. The results of these tests have shown that the silicon die is the origin of long glitches. Two hypotheses have been put forward to explain the heat propagation from the silicon die to the NTD thermometer: ballistic phonon propagation and ionization. In order to distinguish between these two effects we performed a test by breaking the  $\text{Si}_3\text{N}_4$  legs supporting the absorber (65 % of the legs were severed) in order to reduce the ballistic heat transport by a measurable factor.

In the next subsections we give the principal results of each test motivating the physical interpretation of glitches in HFI data discussed in Sect. 7.

### 5.1. Particles on HFI detectors

In the range of energies of interest, the major interaction between particles and materials is ionization. The value  $\Delta E/\Delta x$  versus particle energy is given by the total stopping power curves for silicon, germanium, and copper, and corresponds to the sum of the electronic stopping (inelastic collisions between bound electrons in the solid medium and the ion moving through it) and the nuclear stopping (elastic collisions between the ion and atoms in the sample, almost negligible in the range of energies of interest). In Table 2, we present the energies absorbed in the relevant elements of a bolometer module from  $\alpha$  particles and protons at normal incidence.

### 5.2. TANDEM accelerator test

This test was performed in December 2010 at IPN (Institut Physique Nucleaire – University of Paris-sud) using the TANDEM accelerator.<sup>5</sup> The TANDEM accelerator can produce 23 MeV protons with beam of about 2.5–3 cm always orthogonal

<sup>3</sup> <http://ipnweb.in2p3.fr/tandem-alto/>

<sup>4</sup> Electrons ejected from matter by ionizing radiation.

<sup>5</sup> TANDEM accelerates ions by applying an electrostatic field with a feature of supplying high voltage in the middle of accelerating tube. It can accelerate ions in two steps: first, accelerating negative ions and

**Table 3.** Calibration factors for the 217 GHz SWB, measured under various operating conditions

	Run 1	Run 2	Run 3	Run 4
$T_{\text{plate}}$ [mK]	80	80	80	80
$F_{\text{mod}}$ [Hz]	200	90	182	90
$I_{\text{bias}}$ [nA]	0.2	0.4	0.4	0.2
Cal-fact [ $\mu\text{V}/\text{keV}$ ]	67.5	20.0	28.0	42.2

to the detectors. This means that the beam covers the full surface of the bolometer module.

The aim of this test was to obtain a general view of the interaction between protons and the different elements of an HFI bolometer module. We used three spare HFI SWBs. In front of one, at a distance of about 5 mm, we put a  $10\mu\text{m}$  gold shield to test for possible delta-electron production. The second was placed in front of the TANDEM beam without any shield or optics (filters, horns, etc.). The last was used as a reference bolometer.

In Fig. 5, we present the results of the test for the unshielded bolometer. The histogram of maximum glitch amplitude is shown. Two families of events can be isolated. The first family peaks at  $45\mu\text{V}$  and contains 98.5 % of the glitches. The template built by stacking all the glitches of this family (blue curve in Fig. 5C) can be represented by a fit of a two-time-constant model (a faster  $\tau$  at 4 ms and a slower  $\tau$  at about 20 ms). This family is similar to the long glitch family seen within HFI in-flight data. The second family of glitches peaks at about 0.15 mV and contains about 1.5 % of the glitches. These glitches show reasonable agreement with a template fitting with a single time-constant model with the same time-constant as faster as the first glitch family (red curve on Fig. 5 - C). This family of glitches is similar to the short glitch family seen in HFI in-flight data. The limited integration time of TANDEM experiment did not provide signal to noise sufficiently high enough to allow a confident fitting of the longer time-constants, as is observed in HFI in-flight data. All the glitches have rising times faster than the sampling of the AC read-out electronics so, in most cases the peaks correspond to the first sampled glitch data point.

The bolometer with a gold shield shows the same results as the one without the shield. It seems that we are not able to observe any delta electrons under these conditions.

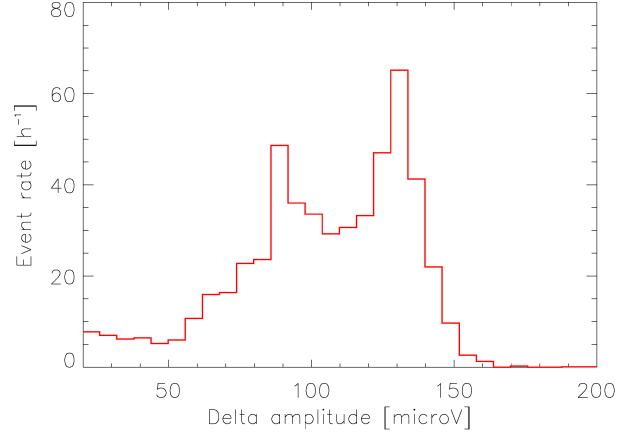
We can summarize the results of the TANDEM accelerator test as:

- We are able to isolate long glitches and short glitches without introducing any delta electrons production process.
- The two families of glitches show the same rate ratio and the same time-constants as observed in HFI data in-flight.
- Slow glitches were not observed as we did not use PSB bolometers during this test.

### 5.3. Alpha-particle tests

These tests were performed between June 2011 and April 2013 using the same 100 mK dilution cryostat and read-out electronics as were used in the TANDEM test. The aim of these tests was to characterize in detail the long glitches observed in HFI data in flight. The TANDEM accelerator tests have demonstrated that

second, further accelerating positive ions after transforming negative ions into positive in the high-voltage terminal ( $E = (q + 1)V$  [MeV]).

**Fig. 6.**  $^{55}\text{Fe}$  X-ray calibration run. Event rate versus signal. The distribution is asymmetric and that two overlapping peaks are present.

it is possible to have long glitches without involving any delta-electron creation processes. Several tests were conducted, as described in the following subsections.

#### 5.3.1. Calibration run

We used a  $^{55}\text{Fe}$  source producing X-rays at 5.9 keV. A typical spectrum (event rate versus signal) is presented in Fig. 6. We can see that the distribution is asymmetric and that two overlapping peaks are present. This distribution can be interpreted as follows. The probability that a 5.9 keV X-ray is absorbed by  $1\mu\text{m}$  of silicon nitride is about 3.5 %. If absorbed in the grid, the 5.9 keV X-ray will ionize the atoms of the silicon nitride. Some of the photoelectrons produced will be absorbed in the silicon nitride itself, so this energy will be fully transformed into heat. Nevertheless, as the grid is  $1\mu\text{m}$  thick, we expect to have a significant rate of photoelectron escape that will produce an asymmetry in the spectrum at lower signals. In addition, at the atomic level, when a core electron is removed leaving a vacancy, an electron from a higher energy level may fall into the vacancy, resulting in a release of energy. This energy can be released in the form of a fluorescence X-ray (for the silicon  $K\alpha/\beta$  fluorescence X-ray of 1.8 keV) or the energy can be transferred to another electron and ejected via the Auger effect. The Auger electrons will be absorbed very quickly in the silicon nitride so in this case all the 5.9 keV of the  $^{55}\text{Fe}$  X-ray will be fully transformed into heat and then measured by the NTD as a change of temperature. This represents the bigger peak in the spectrum at higher energy. If the absorption process produces fluorescence X-rays of 1.8 keV (yield of about 5 %), they will be able to escape easily from the silicon nitride, removing 1.8 keV of the energy to be transformed into heat. This represents the second overlapping peak at lower energy. In conformity with this interpretation we chose to derive the calibration factors in the higher energy peak. Calibration factors (in  $\mu\text{V}/\text{keV}$ ) have been calculated for several conditions (see Table 3).

#### 5.3.2. Delta electron test

In this test, the  $\alpha$  source was put in front of the bolometer with a 2.5 mm diaphragm at a distance of about 1 cm. A  $10\mu\text{m}$  thick

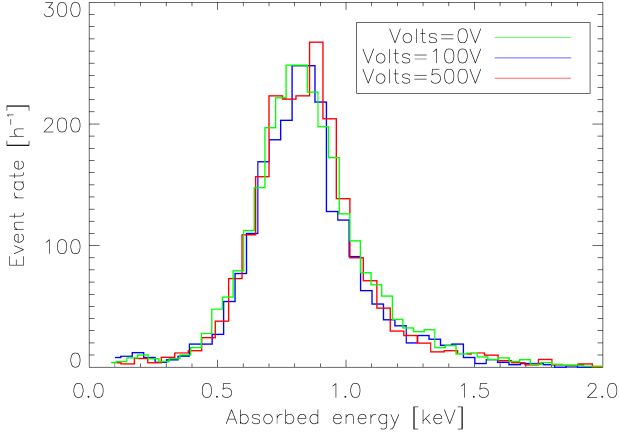


**Fig. 7.** Delta electron test: number of events per hour versus signal, with three different applied voltages.

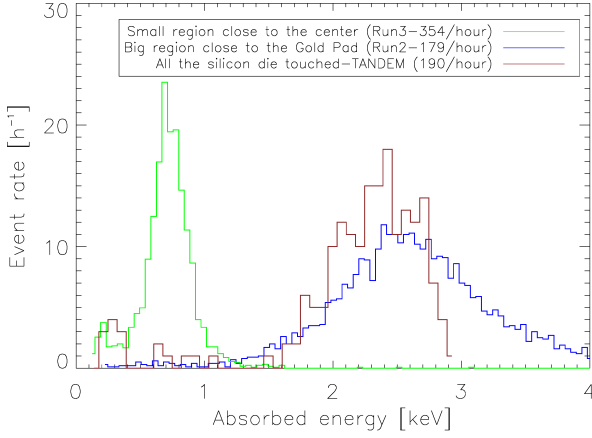


**Fig. 8.** Silicon die tests. Number of events per hour versus calibrated absorbed energy in the NTD thermometer for two positions of the diaphragm along the silicon die (green and blue) and for the TANDEM test (brown). The absorbed energies have been corrected taking into account the differences of the absorbed energy in the silicon die between the tests (1.1 MeV absorbed in the silicon die by  $\alpha$  particle in Grenoble tests and 1.6 MeV absorbed in the silicon die from the TANDEM accelerator test.)

copper shield is glued onto the diaphragm. After interacting with the shield, the  $\alpha$  particles retain an energy of about 1.1 MeV. In this case, the beam spread permits the  $\alpha$  particles to reach both the NTD+absorber and the silicon die. We biased the source and the copper shield with a variable positive voltage from 0 V to 500 V in order to suppress (or partially suppress) the contribution from delta electrons pulled out of the shield. In Fig. 7, we present the histograms of the number of counts versus absorbed energy for the three applied voltages. The three histograms are centred at about the same value. We conclude that the ground-based tests did not show any measurable production of delta-electrons.

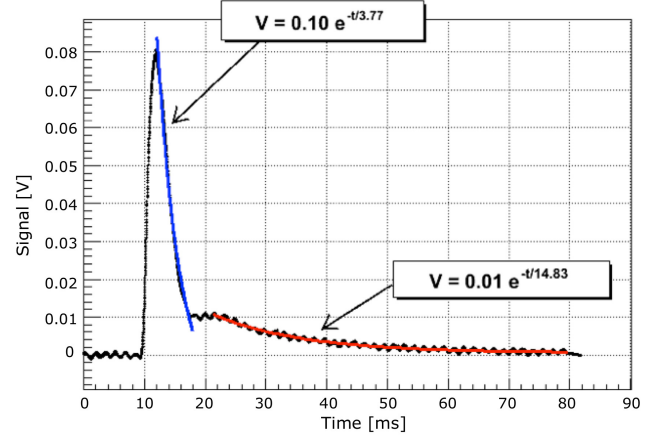


**Fig. 9.** Silicon die tests. Glitch template built by stacking 466 events coming from impacts in the Si wafer (black curve). The fitted time-constants with exponential models are presented (blue and red curves).

### 5.3.3. Silicon die tests

In this test, the  $\alpha$  source was put in a variety of positions in front of the silicon die. We used a 1.5 mm diaphragm with  $10\mu\text{m}$  cooper shield at a distance of about 5 mm from the NTD thermometer. In this case, the  $\alpha$  particles can interact only with the silicon die. The 1.1 MeV  $\alpha$  particle is completely absorbed in the silicon die. We define the attenuation factor  $E_{die}/E_{bolo}$  as the ratio of the energy absorbed per glitch in the silicon die to the energy absorbed in the NTD thermometer. In this test we checked the variation of the attenuation factor by moving the source between two positions along the silicon die. In Fig. 8 we present the comparison between the energy distribution of the TANDEM test (in brown) and the histograms corresponding to the two positions of the diaphragm. The green line corresponds to a little region of the silicon die close to the absorber. The blue line corresponds to larger region close to the gold pad. The attenuation factor can change from about 500 to 1000 between the two positions. In the case of TANDEM test, where the silicon die is fully covered by the proton beam, the derived attenuation factor is 650.

In parallel with the tests that use the HFI read-out electronics, we performed several tests dedicated to the characterization of the interaction of particles with the silicon die using DC read-out electronics operating at ambient temperature without using cold JFETs. This electronics chain has been validated by the IAS team for testing scintillating bolometers (Coron et al. 1990). The noise of the readout was about  $11\text{ nV Hz}^{1/2}$ , low enough to have a good signal-to-noise ratio on the glitches.

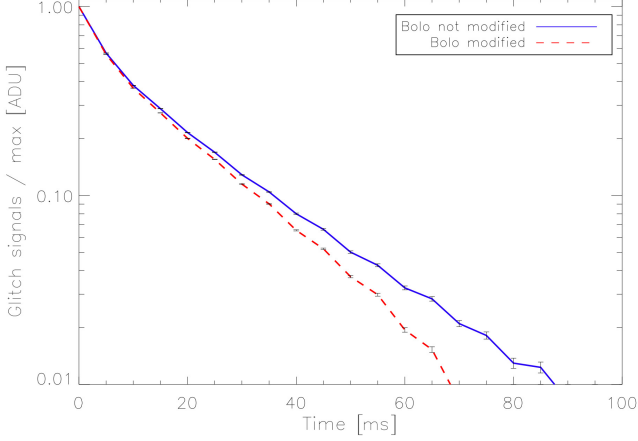
The aim of these tests was to sample fast enough to be able to distinguish different physical processes that might be implicated in the heat propagation from the silicon die to the NTD thermometer. The results of this test are in agreement with the Grenoble and TANDEM accelerator tests. In Fig. 9 we present a typical glitch produced from the hit of an  $\alpha$  particle in the silicon die, along with the time-constants of an exponential model.

### 5.3.4. Modified bolometer test

This test was designed to demonstrate the ballistic phonon propagation from the silicon die to the grid + NTD thermistor. To achieve this goal we broke the grid legs (65 % of the leg cross-

**Table 4.** Effect of removing legs from an SWB: two-time-constant model parameters. The errors include systematic effects between the two runs.

	$\text{Amp}_{\text{fast}} [\%]$	$\tau_{\text{fast}} [\text{ms}]$	$\tau_{\text{slow}} [\text{ms}]$
Unmodified SWB	$46 \pm 2.1$	$4.0 \pm 0.8$	$20.0 \pm 1.9$
Modified SWB	$37 \pm 2.6$	$3.6 \pm 0.9$	$18.9 \pm 1.9$

**Fig. 10.** Normalized template of the hit on the silicon die. Error bars show statistical errors only.

sectional area was severed) in order to reduce the ballistic heat transport by a measurable factor. The nitride legs were broken using a stainless steel needle. The break location was made right at the edge of the Si frame. The breaks were made by placing the needle next to the leg and also with the needle next to the Si frame. The needle was then pushed sideways to break the legs.

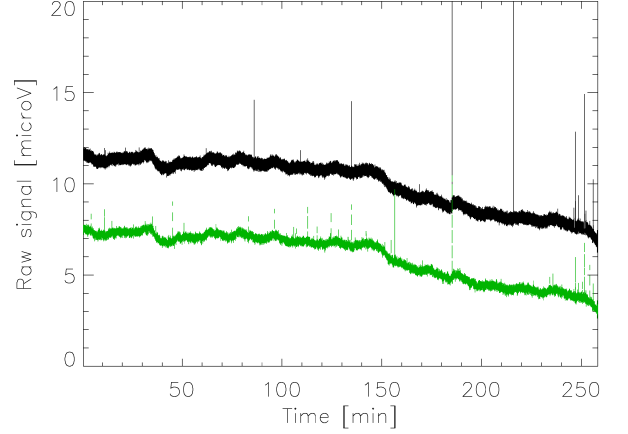
We performed an initial reference test with the unmodified bolometer. Then we performed the test with the modified bolometer, using the same setup. The spectrum of the count rate versus the calibrated energy absorbed showed that there was no change in the measured energy or the counts. We did, however, observe a difference in glitch shape between the two runs. We built a template by stacking all the events coming from silicon die hits. We fitted these templates with a two-time-constant model (Fig. 10 and Table 4). The amplitude corresponding to the fast time-constant has changed by about 20 %. This result is consistent with the hypothesis that part of the the heat propagates to the NTD thermometer by ballistic phonons.

### 5.3.5. Coincidence test

For this test we used a PSB bolometer. The  $\alpha$  source was put in front of the grids of the PSB using a 1.5 mm diaphragm with 10  $\mu\text{m}$  copper shield at a distance of about 5 mm from the NTD thermometer. A PSB bolometer module is surrounded by copper except for a 1.59 mm hole in front of the grids and a small aperture on the silicon die, so in this case, we were completely sure to hit only the grids.

The coincidence of short glitches on PSBA and PSBb seen in flight (Planck Collaboration (2013 results X) 2014) show that approximately 50 % of events are seen in both PSBA and PSBb with no phase shift and with no correlation in amplitude. Modelling the interaction of hundreds MeV protons with 1  $\mu\text{m}$  silicon nitride with GIANT-4<sup>6</sup>, we found that about ten electrons can be

<sup>6</sup> <http://wwwasd.web.cern.ch/wwwasd/geant/rd44.html>

**Fig. 11.** HFI ground calibration. 4 hours of time-ordered data (TOD) taken under stable environmental conditions. *Black*: PSBa. *Green*: PSBb.

ejected from one grid producing a small change in temperature on the other NTD below the detection threshold. The rate of 50% correlation can be explained by geometrical effects such as particles coming from the top or bottom. Glitch PSBa/b coincidences which do have strong amplitude correlation, on the other hand, corresponding to direct impact of protons on the two grids, have been observed from 2 % to 4 % depending on the bolometer.

These ground-test results give a level of coincidence of about 3% for glitches that are very well correlated in amplitude, when considering only the glitches detected at or above  $5\sigma$ . This is in agreement with direct interactions of  $\alpha$  particles with the two grids. We observed a low level of glitches without a strong amplitude correlation, but the integration time of these tests was insufficient to show the expected 50 % level of coincidence due to ejected electrons. We conclude that ground-based coincidence tests did not fully explain the coincidence level between PSB bolometers observed in flight. For a complete analysis of this issue we refer to the companion paper (Planck Collaboration (2013 results X) 2014).

### 5.4. HFI ground calibration

During pre-launch *Planck* system tests, CRs were seen by HFI, but at a much lower rate than at L2. At sea level, muons are the most numerous charged CR particles, with a mean energy of about 4 GeV (Ramesh et al. 2012). The integral intensity of vertical muons at sea level is about  $1 \text{ cm}^{-2} \text{ min}^{-1}$  for horizontal detectors. The overall angular distribution of muons at the ground is proportional to  $\cos^2 \delta$ , where  $\delta$  is the elevation angle.

During the CSL ground-based tests, the focal plane is almost vertical so we expect to have few tens of events per hour in the silicon die and few per day in the absorber + NTD. The absorbed energy in the silicon die is about 150 keV, so considering the attenuation factor measured in the Grenoble tests, muons are expected to produce measurable glitches during the pre-launch HFI calibration tests. In addition, in the PSB bolometers, these glitches should be seen in coincidence.

To demonstrate the glitch rate observed during HFI ground calibration testing, Fig. 11 shows a typical PSB that we observed under stable condition during the HFI ground calibration experiments.



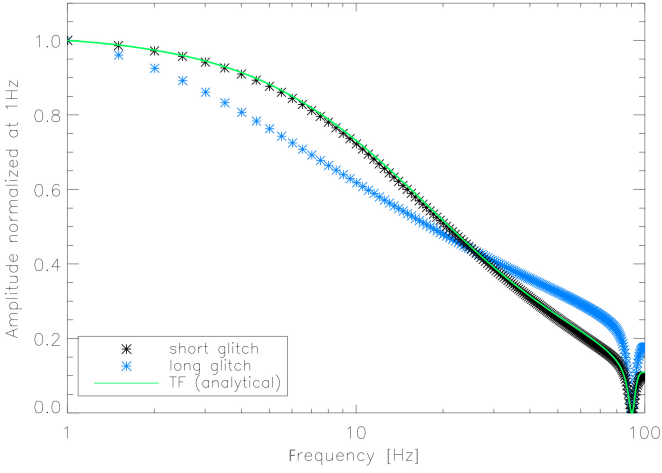


**Fig. 12.** Comparison of the HFI optical transfer function (Planck Collaboration (early results IV) 2011) (green line), short glitch templates (black stars), and long glitch template (blue stars).

We saw about 20 glitches per hour in PSBb (green curve) and fewer in PSBa (black curve). In all the polarized bolometers, the ratio of the PSBa counts to the PSBb counts is the same; almost all the events seen in PSBa are in coincidence with an event seen in PSBb.

## 6. Discussion

### 6.1. Short glitches

Short glitches dominate the rate at high energies. This has been confirmed in the ground-based tests (see, e.g., Fig. 5). The thermal response template built from this family is in a good agreement with in-flight HFI bolometer data and ground-based data on direct interaction of particles with the absorber and NTD thermometer. The energy distribution of the short glitches is similar in all the bolometers and shows a double-peaked structure (Planck Collaboration (2013 results X) 2014). The bump in the short glitch distribution, centered at about 20 keV, is completely consistent with the interaction between CRs and the NTD thermometer. At low energies, the distribution corresponds to the interaction between the absorber and the CRs.

Another indication that short glitches are produced from direct interaction between CRs and the grid or thermistor can be found in the comparison between the HFI bolometer electronics time response measured on sky signal (Planck Collaboration (early results IV) 2011) and the transfer function built from the short glitch template (see Fig. 12). The agreement between the ground and planet-based transfer function (solid green) and short glitches (black stars) is good, considering that the template is constructed independently of any model. We can conclude that the HFI short glitches are produced by direct interaction of particles with one of the absorber grids (or directly with the NTD thermistor for a small subset of them).

### 6.2. Long glitches

By contrast, the long glitch template (blue stars in Fig. 12) is not consistent with the optical transfer function, indicating a different physical origin for these glitches.

Two hypothesis have been put forward to explain the large number of long glitches seen in HFI flight data: (1) the NTD thermometer is sensitive to a change in temperature of other (larger) elements; or (2) long glitches come from indirect interaction between CRs and bolometers. From the ground-based tests we determined that it is not possible to generate a number of delta-electrons large enough to reproduce the energy distribution of HFI in-flight long glitches (Fig. 4). On the other hand we have shown that the NTD thermometer is sensitive to temperature changes of the silicon die. All the ground-based tests have confirmed this hypothesis. In addition, the HFI ground-based calibration data show a rate of events compatible with the CR flux at sea level over the silicon die surface. Starting from these considerations, we have developed a toy model of the impact of CRs with the silicon die in orbit at L2 that can explain the long glitch spectrum seen by the *Planck* HFI during flight observations. The details of this model are presented in (Planck Collaboration (2013 results X) 2014).

The physical interpretation of long glitches can be found in the shape of the long glitches that we have isolated during the ground-based tests. With the improved temporal resolution due to the faster DC-based REU readout electronics and sampling, we can clearly see (Fig. 9) the dual time-constant response that results from heat transfer between the silicon die and the NTD thermometers. We identify two possible hypotheses to explain the heat propagation from the silicon die to the NTD thermometer:

**Ionization and thermal diffusion:** According to this hypothesis, the faster time-constant is given by ionization within the silicon die. The ionization signal is obtained by the collection of the electron-hole pairs created by interaction of  $\alpha$  particles in the silicon crystal via the gold pad. The long tail can still be explained by the heat diffusion between the silicon die and the NTD thermometers. Using the bolometer parameters we can determine the equivalent bias step amplitude needed to produce a glitch of about 4 keV (the typical energy absorbed in the bolometer from a hit in the silicon die). We obtain  $\Delta I_b = 0.2$  nA, which is of the same order as the working bias current. If present, an effect as strong as this should be evident through inspection of the raw TOI signals. In fact, before sufficient time has elapsed for heat diffusion within the bolometer, a collected charge must show a peak in the raw signal with a decay time constant determined only by the RC time-constant of the individual detector readout circuitry. The sign of this peak should not change with the changing polarity of the detector bias current. Therefore, this effect should be easily distinguished from a thermal glitch. The results of this analysis are presented in Fig. 13: in black we show a template of the typical unperturbed raw signal set during the test. The red and the blue curves represent the difference between a raw signal with a glitch (in the center of the half periods) and the template. There is no evidence of ionization in the raw signals; all the glitches can be fully explained by pure thermal events (i.e., “hot” and/or “cold” phonons).

**Ballistic phonon propagation and thermal diffusion:** According to this hypothesis, the faster time-constant, which corresponds to the typical time-constant of the bolometers as measured with optical sources in ground and flight calibration testing, can be explained by ballistic phonon heat conduction:<sup>7</sup>

<sup>7</sup> Ballistic conduction is the unimpeded flow of energy carrying charges over large distance scales within a material.

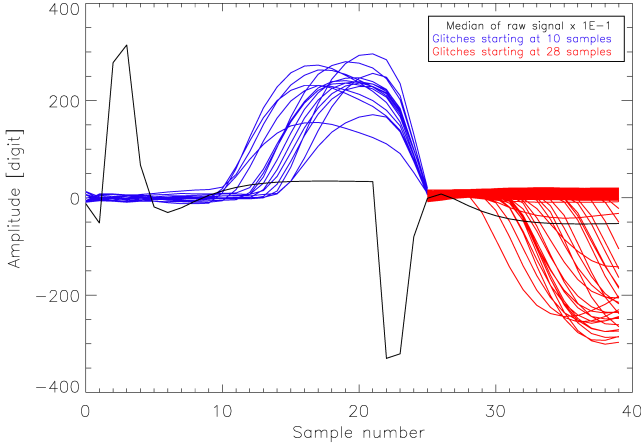


**Fig. 13.** Raw signal analysis: the black curve represent the template of the typical unperturbed raw signal set during the test. The red and the blue curves represent the difference between a raw signal with a glitch (in the center of the half periods) and the template.

in our case ballistic phonons can propagate from the silicon die and up the grid legs unimpeded, depending on the geometrical coupling fixed by the size and the number of the legs. The final effect is equivalent to a particle absorbed directly in the grid.

The longer time-constant (tens of milliseconds) represents the non-ballistic thermal heat diffusion between the silicon die and the NTD thermometers. This implied time-constant is consistent with the heat capacitance of the silicon die and the thermal conduction of the silicon die to the bolometer itself. A detailed thermal model of the bolometer is presented in a companion article (Spencer et al. in preparation) that describes ground-based tests on flight-spare bolometers conducted in Cardiff. The tests were performed by placing NTD-Ge thermometers and 100 k $\Omega$  heaters at various locations on a bolometer module (the silicon die, the PWB, and the module housing). Glitch events were simulated by rapid injection of known quantities of thermal energy through the additional resistors attached to the bolometer module, while observing the temperature response of the bolometer and its elements.

The modified bolometer tests of this work have shown that by breaking 8 of the 12 grid-support legs we can reduce the amplitude of the long-glitch fast time-constant amplitude, without an accompanying decrease in the glitch long-tail contribution. This implies a reduced effective ballistic cross-sectional area between the silicon die and spider-web absorber/NTD. This is in complete agreement with the ballistic conduction hypothesis.

### 6.3. Slow glitches

Slow glitches are the rarest glitch events we see in the HFI in-flight bolometers. They affect only the PSBa and have a rate of a few per hour in flight. The energy distribution of the slow glitches shows the same power law index as the energy distribution of long glitches (see Fig. 4). In addition, the slow glitches share the template of the long glitches, but without the component with the shortest time constant. The slow glitches were not reproduced during any of the HFI ground-based tests, both pre-launch with the HFI focal plane unit (FPU), and post-launch with flight-spare hardware. In light of this fact, we are limited to

proposing a hypothesis for the origin of the slow glitches that is consistent with our current results but lacks experimental confirmation. The presence of the feed-through (see Sect. 3) connecting the PSBa bolometer to its corresponding silicon die is the only difference between the PSBa bolometers and the other types of bolometers in HFI (PSBb and SWB). The PSBa feed-through elements have a strong thermal coupling with the silicon die and gold pad. A proton hitting a PSBa feed-through, therefore, can heat the corresponding silicon die to produce heat diffusion from the silicon die to the NTD thermometer. This heating would not have the corresponding ballistic heat conduction associated with a silicon die/CR glitch event, and therefore no fast time-constant would be observed. The differences in the effective surface area of the feed-throughs with respect to the corresponding silicon dies, of a factor of about 100, may explain the differences in the rate between the long glitches and the slow glitches.

## 7. Implications for future space missions

*Planck* HFI has demonstrated the effectiveness of using a grid absorber rather than a solid/bulk absorber for collecting CMB photons, while drastically reducing the number of direct glitches (short glitches). This characteristic allowed HFI to deliver data at the signal-to-noise ratio required for the *Planck* scientific goals. Nevertheless, we observed a larger than expected number of glitches at low energies (long glitches). The ground-based experiments discussed in this paper have demonstrated that the silicon die is able to propagate the energy absorbed from CRs to the bolometer absorber and NTD thermometer. In this case the absorbed energy propagates to the NTD thermometer via ballistic phonons; this is followed by a contribution of thermal diffusion from the silicon die to the absorber and NTD.

The study of the physical processes related to athermal propagation and ionization in a crystal, and more generally the effects of particles in cryogenic bolometers, have several applications, including new-generation space missions at millimetre and submillimetre wavelengths (e.g., Caserta et al. 1990), high resolution X-ray spectrometry (e.g., Kelley et al. 2007; Kilbourne et al. 2006; Stahle et al. 2004), and direct detection of dark matter (e.g., Sundqvist 2008; Martineau et al. 2004). In this section we discuss in particular how our results can be used to improve the design of new arrays of millimetre detectors for future space missions such as SPICA-SAFARI (Goicoechea et al. 2011; Spinoglio et al. 2011), PIXIE (Kogut et al. 2011), and CORE (CORE Team 2011).

The goal of improving the noise-equivalent power (NEP) of new experiments by at least one order of magnitude (from  $10^{-17}$  W Hz $^{-1/2}$  to  $10^{-18}$  W Hz $^{-1/2}$ ), can be achieved by increasing the focal plane coverage, using thousands of background-limited instrument performance (BLIP) contiguous pixels.<sup>8</sup> Each pixel of these arrays must be micromachined starting from a common substrate.

Two new generation of detectors other than classical high impedance bolometers are in competition in the development of future millimetre space missions. We summarize their principal characteristics and discuss how to minimize the effect of particle impacts.

Transition Edge Sensors (TES) are thermal detectors which use a superconductor thermometer biased at the superconductor

<sup>8</sup> The sensitivity of bolometers is fundamentally limited by statistical fluctuations of the radiation power coming from observed source and thermal emission from the cryogenic stages of the instrument.

transition ( $R_{\text{mean}} \sim 10 \text{ m}\Omega$ ) (e.g., Piat et al. 2002; Hubmayr et al. 2009). The only conceptual difference between the HFI high-impedance bolometers and TES bolometers is the sensitive element used to measure the change in temperature, which is a superconducting element in TES. Direct CRs impacting TES pixels will have the same effect as in the high-impedance bolometers. However, in TES arrays, because of the common silicon wafer, the ballistic phonons and thermal heat transport from the wafer to the thermometer will affect several detectors at the same time. This effect could be reduced by, e.g., increasing the heat capacity of the substrate and/or directing the ballistic phonon leak towards the housing rather than to the pixels.

Kinetic Inductance Detectors (KIDs) are superconducting resonant elements electromagnetically coupled to a common read-out transmission line. The absorption of the incoming photons causes a change of the resonance frequency through the breaking of Cooper pairs. The main advantages of KIDs over TES arrays are the straightforward frequency multiplexing readout and a faster time response (always  $< 1 \text{ ms}$ ). Another conceptual difference is that KIDs are insensitive to a change of base temperature provided that  $T_{\text{base}} \ll T_c$  (where  $T_c$  is the superconductivity critical temperature). Considering an absorber of the same geometry as TES bolometers (suspended grid structure), the effect of particles in KIDs will be reduced by a factor between 10 and 100 due to the (still poorly understood) capability of ballistic phonons to break Cooper pairs. Only phonons with energy exceeding the superconducting gap can break pairs and produce a measurable signal. The presence of such energetic ballistic phonons could be attenuated, as in the case of TES detectors, by increasing the leak of energy towards the housing. Work is in progress on this subject (Swenson et al. 2010; Moore et al. 2012; Cruciani et al. 2012).

## 8. Conclusion

In this paper we have described several ground-based tests that lead to a physical interpretation of the impact of CR collisions on the *Planck* HFI bolometers in flight. An analytical model has been developed in order to validate the physical interpretation with both ground-based and in-flight data. We have shown that:

- The dominant component of the in-flight long glitches is produced by the impact of CRs on the silicon wafer that supports the absorber and the NTD thermometer. The heat propagates to the NTD thermometer by ballistic phonons followed by a contribution of thermal diffusion.
- Short glitches are produced by direct interaction of a particle with either the absorber grid or the NTD-Ge thermistor. In the case of PSB detectors, short glitches may also be the result of secondary electrons from a short glitch induced by a CR in the other PSB detector of the pair.
- Slow glitches have not been reproduced in the ground-based tests. Their physical origin is consistent with the hypothesis that slow glitches result from the impact of CRs on the feed-through of the PSBa bolometers, but further work is needed to definitively identify their origin.
- The influence of CR/detector glitches on scientific data quality should be included as a design constraint for future-generation detector arrays for space applications. This should be included in parallel with all of the other characteristics such as detector NEP and time response. In particular, optical beam-response tests should be planned to study

irradiation on complete detector arrays (e.g., pixels, substrate, and housing). Starting from the same design conditions (for example, size and shape of the absorber, substrate and thermal contacts), non-thermal detectors such as KIDs may present a conceptual advantage.

## References

- Adriani, O., Barbarino, G. C., Bazilevskaya, G. A., et al. 2011, *Science*, 332, 69
- Caserta, A., Bernardis, P. D., Masi, S., & Mattioli, M. 1990, *Nuclear Instruments and Methods in Physics Research A*, 294, 328
- Catalano, A., Coulais, A., & Lamarre, J.-M. 2010, *Appl. Opt.*, 49, 5938
- Christian, E. R., Bravar, U., de Nolfo, G. A., Ryan, J. M., & Stochaj, S. 2011, AGU Fall Meeting Abstracts, B2017
- CORE Team. 2011, [http://www.core-mission.org/documents/CoreProposal\\_Final.pdf](http://www.core-mission.org/documents/CoreProposal_Final.pdf)
- Coron, N., Artzner, G., Leblanc, J., Jegoudez, G., & de Marcillac, P. 1990, in 9th Moriond Astrophysics Meeting, ed. J. Audouze & J. Tran Thanh Van, 275–288
- Cruciani, A., Swenson, L. J., Monfardini, A., et al. 2012, *Journal of Low Temperature Physics*, 167, 311
- Gaertner, S., Benoit, A., Lamarre, J.-M., et al. 1997, *A&AS*, 126, 151
- Goicoechea, J. R., Roelfsema, P. R., Jellema, W., & Swinyard, B. M. 2011, in IAU Symposium, Vol. 280, 280th Symposium of the International Astronomical Union, 179P
- Holmes, W. A., Bock, J. J., Crill, B. P., et al. 2008, *Appl. Opt.*, 47, 5996
- Hubmayr, J., Aubin, F., Bissonnette, E., et al. 2009, arXiv:0908.1997
- Jones, R. C. 1953, *Journal of the Optical Society of America* (1917-1983), 43, 1917
- Kelley, R. L., Mitsuda, K., Allen, C. A., et al. 2007, *PASJ*, 59, 77
- Kilbourne, C. A., Boyce, K. R., Brown, G. V., et al. 2006, *Nuclear Instruments and Methods in Physics Research A*, 559, 620
- Kogut, A., Fixsen, D. J., Chuss, D. T., et al. 2011, *J. Cosmology Astropart. Phys.*, 7, 25
- Leske, R. A., Cummings, A. C., Mewaldt, R. A., & Stone, E. C. 2011, *Space Sci. Rev.*, 126
- Martineau, O., Benoît, A., Bergé, L., et al. 2004, *Nuclear Instruments and Methods in Physics Research A*, 530, 426
- Masi, S., Battistelli, E., de Bernardis, P., et al. 2010, *A&A*, 519, A24
- Mather, J. C. 1982, *Appl. Opt.*, 21, 1125
- Mauskopf, P. D. 1997, PhD thesis, University of California, Berkeley
- Mewaldt, R. A., Davis, A. J., Lave, K. A., et al. 2010, *ApJ*, 723, L1
- Mohammadzadeh, A., Evans, H., Nieminen, P., et al. 2003, *Nuclear Science, IEEE*, 50, 2272
- Moore, D. C., Golwala, S. R., Bumble, B., et al. 2012, *Applied Physics Letters*, 100, 232601
- Piat, M., Lagache, G., Bernard, J.-P., Giard, M., & Puget, J.-L. 2002, *A&A*, 393, 359
- Picozza, P., Sparvoli, R., Adriani, O., et al. 2011, in *Particle Physics at the Year of Astronomy*, ed. H. Fritzsch, K. K. Phua, c.-e. B. E. Baaquie, A. H. Chan, N.-P. Chang, S. A. Cheong, L. C. Kwek, & C. H. Oh, *Il Nuovo Cimento*, 200–206
- Planck Collaboration (2013 results I). 2014, *A&A*, in press, [arXiv:astro-ph/1303.5062]
- Planck Collaboration (2013 results X). 2014, *A&A*, in press, [arXiv:astro-ph/1303.5071]
- Planck Collaboration (early results IV). 2011, *A&A*, 536, A4
- Planck Collaboration (early results VI). 2011, *A&A*, 536, A6
- Ramesh, N., Hawron, M., Martin, C., & Bachri, A. 2012, ArXiv e-prints
- Rieke, F. M., Lange, A. E., Beeman, J. W., & Haller, E. E. 1989, *Nuclear Science, IEEE*, 36, 946
- Spinoglio, L., Magliocchetti, M., Gruppioni, C., Franceschini, A., & Isaak, K. 2011, in *Astronomical Society of the Pacific Conference Series*, Vol. 446, *Galaxy Evolution: Infrared to Millimeter Wavelength Perspective*, ed. W. Wang, J. Lu, Z. Luo, Z. Yang, H. Hua, & Z. Chen, 11
- Stahle, C. K., Boyce, K. R., Brown, G. V., et al. 2004, *Nuclear Instruments and Methods in Physics Research A*, 520, 472
- Stone, E. C. 2012, in EGU General Assembly Conference Abstracts, Vol. 14, EGU General Assembly Conference Abstracts, ed. A. Abbasi & N. Giesen, 3933
- Sudiwala, R. V., Maffei, B., Griffin, M. J., et al. 2000, *Nuclear Instruments and Methods in Physics Research A*, 444, 408
- Sundqvist, K. 2008, in APS March Meeting, 35015
- Swenson, L. J., Cruciani, A., Benoit, A., et al. 2010, *Applied Physics Letters*, 96, 263511
- Vaillancourt, J. E. 2005, *Review of Scientific Instruments*, 76, 043107